Ondes Gravitationnelles, Séminaire Poincaré XXII (2016) 87 – 105 Séminaire Poincaré

Exploring the Universe with Gravitational Waves

Michele Maggiore
Département de Physique Théorique and Center for Astroparticle Physics
Université de Genève
24 quai Ansermet
CH–1211 Genève 4, Switzerland

Abstract. With the recent detections of GW150914 and GW151226 we have entered the era where we can begin to use gravitational waves (GWs) to explore the Universe. We will give a short overview of two mechanisms of GW production that can give information unaccessible by electromagnetic observations. Namely, we will discuss GW emission by quasi-normal modes of black holes, as well as stochastic GW backgrounds produced in the early Universe.

1 Introduction

The first direct detection of a GW event, GW150914, took place on Sept. 14, 2015, when the Hanford and Livingston interferometers of the LIGO Observatory, at the very beginning of the first science run in the advanced LIGO configuration, detected the GWs emitted by the coalescence of a BH-BH binary. The result was announced by the LIGO and Virgo collaborations on Feb. 11, 2016 [1–4] and represented the culmination of efforts which had lasted for over 50 years, from a whole community. During this first scientific run of the LIGO detectors, which continued until Jan. 2016, a second confirmed BH-BH coalescence, GW151226, was detected on Dec. 26, 2015. It was then announced in June 2016, together with a third plausible event, whose statistical significance was however not sufficient to claim a third discovery [5]. The advanced LIGO detectors have not yet reached their target sensitivity, and will alternate data-taking periods with commissioning periods. To have an idea of the discovery potential at design sensitivity one can observe that GW150914, which was detected at a combined signal-to-noise ratio $\hat{\rho} \simeq 22.7$ (corresponding to a significance higher than 5.3σ [6]), at design sensitivity would have been observed with a signal-to-noise ratio $\mathcal{O}(100)$. Advanced Virgo is expected to join data-taking in 2017 and further advanced interferometers, such as KAGRA in Japan and LIGO-India (or "Indigo"), are expected to join later, forming a network of advanced detectors, with even better sensitivities and localization capabilities. Thus, we are indeed entering the era in which we can start to explore the Universe using GWs.

Within the limited scope of my contribution to this Poincaré seminar, I will restrict myself to two selected topics, which are particularly interesting because of their complementarity with electromagnetic (or neutrino) observations. I will first discuss the emission of GWs from quasi-normal modes (QNMs) of black holes. I will then focus on what we know about stochastic backgrounds of GWs. More details on these topics (and a more complete reference list), as well as an exhaustive discussion of sources of GWs, will be presented in the second volume of my textbook on GWs.

The first volume [7], which appeared in 2007, dealt with the theory of GWs (in Part I) and the experiments (Part II). After 10 more years of work, the second volume [8] is now basically finished (and even thicker than Vol. 1!), and should be available by the end of 2017. It will cover astrophysical sources (Part III) and cosmological sources (Part IV).

2 Black hole quasi-normal modes

Black-hole perturbation theory is by now a classic chapter of General Relativity. The subject has a long history, going back to works of Regge and Wheeler (1957), Zerilli (1970), Vishveshwara (1970), Press (1971), Teukolsky (1973), Chandrasekhar (1975,1983), Chandrasekhar and Detweiler (1975) [9–16], and several others. The subject remains extremely active to the present time, both because of the needs of GW astronomy, and because the quasi-normal modes (QNMs) of black holes (BHs) are a natural bridge between classical and quantum gravity, and even play a role in the AdS/CFT correspondence (although these aspects will not be covered in our talk). The subject also has a mathematical elegance, and I hope that it will be interesting for the more mathematical part of the audience.

The fact that an elastic body, such as a rod or a string, has a set of normal modes, is familiar from elementary mechanics and from every-day experience. It is however much more surprising to discover that a BH is also characterized by a set of normal modes (or, as we will see, more precisely, by quasi-normal modes). A BH is a pure space-time configuration, with no matter left to sustain oscillations. These QNMs are therefore proper vibration modes of space-time itself. A BH with a given mass and angular momentum is characterized by an infinite set of such modes, with calculable frequencies and damping times, into which it will 'ring' when it is excited by an external perturbation, in order to get rid of the excess energy and settle down to its equilibrium Kerr configuration. In the following we will see how these quasi-normal modes emerge. For reasons of space, we will not discuss here the normal modes of neutron stars, where the interplay between space-time and matter oscillations makes the issue more complex, and which can be used to infer properties such as the equation of state (EOS) of neutron stars. We will only give here the main results. Detailed derivations, as well as a much more complete list of references, will be provided in [8]. Several excellent reviews on QNM of BHs and neutron stars also exist, see in particular [17–19].

2.1 Scalar perturbations in a BH background

Before moving to the study of gravitational perturbations of BHs, let us consider scalar perturbations in a BH background. In a spacetime with background metric $\bar{g}_{\mu\nu}$, a massless scalar field ϕ obeys the wave equation

$$\Box\phi \equiv (-\bar{g})^{-1/2}\partial_\mu\left[(-\bar{g})^{1/2}\bar{g}^{\mu\nu}\partial_\nu\right]\phi = 0\,, \tag{1}$$

where $\bar{g}$ denotes the determinant of $\bar{g}^{\mu\nu}$. We consider a Schwarzschild black hole in Schwarzschild coordinates, so the metric is given by

$$ds^2 = -A(r)dt^2 + B(r)dr^2 + r^2\left(d\theta^2 + \sin^2\theta d\phi^2\right)\,, \tag{2}$$

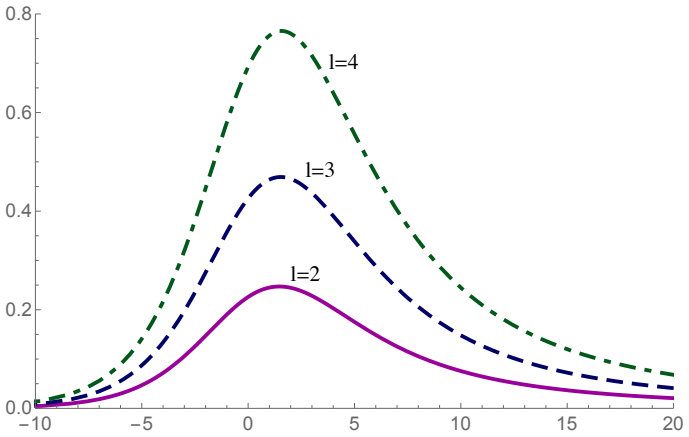

Figure 1: The potential $V[r(r_*)]$ for scalar perturbations, and $l = 2, 3, 4$. We use units $M = 1$, so $R_S = 2$.

where

$$A(r) = 1 - \frac{R_S}{r}\,, \qquad B(r) = \frac{1}{A(r)}\,, \tag{3}$$

and $R_S = 2GM$ is the Schwarzschild radius (we set $c = 1$). Given the spherical symmetry of the background metric, it is convenient to expand $\phi(t, \mathbf{x})$ in spherical harmonics,

$$\phi(t, \mathbf{x}) = \frac{1}{r} \sum_{l=0}^{\infty} \sum_{m=-l}^{l} u_{lm}(t, r) Y_{lm}(\theta, \phi)\,. \tag{4}$$

Inserting this expansion into eq. (1) we get

$$\left[\frac{\partial^2}{\partial r_*^2} - \frac{\partial}{\partial t^2} - V_l(r)\right] u_{lm}(t, r) = 0\,, \tag{5}$$

where

$$V_l(r) = A(r) \left[\frac{l(l+1)}{r^2} + \frac{R_S}{r^3}\right], \tag{6}$$

and r_* is the "tortoise coordinate",

$$r_* \equiv r + R_S \log \frac{r - R_S}{R_S}\,. \tag{7}$$

Observe that r_* ranges from $-\infty$ to $+\infty$ as r goes from the horizon $r = R_S$ to $r = +\infty$. It is convenient to perform a Fourier transform with respect to the time variable, writing

$$u_{lm}(t, r) = \int_{-\infty}^{\infty} \frac{d\omega}{2\pi}\, \tilde{u}_{lm}(\omega, r) e^{-i\omega t}\,. \tag{8}$$

Then $\tilde{u}_{lm}(\omega, r)$ satisfies the equation

$$\left[-\frac{d^2}{dr_*^2} + V_l(r)\right] \tilde{u}_{lm} = \omega^2\, \tilde{u}_{lm}\,. \tag{9}$$

This has the form of a Schrödinger equation in one dimension, defined on the line $-\infty < r_* < \infty$, for a particle of mass m, written in units $\hbar^2/(2m) = 1$, with $V_l(r)$ formally playing the role of the potential and ω^2 formally playing the role of the energy. This formal analogy will be useful in the study of the solutions of this equation. The potential $V_l(r)$ is shown in Fig. 1, as a function of r_*, for $l = 2, 3, 4$. Because of the spherical symmetry of the Schwarzschild metric, $V_l(r)$ does not depend on the index m of u_{lm}.

We must now supplement eq. (5) with the appropriate boundary conditions. Of course, the choice of boundary conditions depends on the physics of the problem. To understand the possible choices and their physical meaning, let us first look at the asymptotic behaviors of the solutions as $r_* \to \pm\infty$. The potential (6) vanishes as $1/r^2$ for large r, so to leading order in $1/r$ eq. (5) becomes a free wave equation. Its solution at $r_* \to +\infty$ will therefore be a superposition of plane waves,

$$u_{lm}(t,r) \to \int_{-\infty}^{\infty} d\omega \, \left[A^{\rm out}_{lm}(\omega) e^{-i\omega(t-r_*)} + C^{\rm in}_{lm}(\omega) e^{-i\omega(t+r_*)}\right] , \qquad (r_* \to +\infty) . \tag{10}$$

The condition that $u_{lm}(t,r)$ is real implies

$$A^{\rm out}_{lm}(\omega) = [A^{\rm out}_{lm}(-\omega)]^* , \qquad C^{\rm in}_{lm}(\omega) = [C^{\rm in}_{lm}(-\omega)]^* . \tag{11}$$

The solution proportional to $\exp\{-i\omega(t-r_*)\}$ is an outgoing radial wave, i.e. radiation escaping to infinity, while the solution proportional to $\exp\{-i\omega(t+r_*)\}$ is an incoming wave, describing radiation coming from infinity toward the black hole.

To determine the possible solutions at $r_* \to -\infty$, we observe that the potential $V_l(r)$ near the horizon vanish as $A(r)$. Near the horizon the relation between r_* and r becomes

$$r_* \simeq R_S + R_S \log \frac{r - R_S}{R_S} , \tag{12}$$

so

$$A(r) \simeq e^{(r_* - R_S)/R_S} , \tag{13}$$

which vanishes exponentially in r_* as $r_* \to -\infty$. Therefore, as $r_* \to -\infty$ we have again a free wave equation, and therefore we find again incoming and outgoing radial waves,

$$u_{lm}(t,r) \to \int_{-\infty}^{\infty} d\omega \, \left[A^{\rm in}_{lm}(\omega) e^{-i\omega(t-r_*)} + C^{\rm out}_{lm}(\omega) e^{-i\omega(t+r_*)}\right] , \qquad (r_* \to -\infty) , \tag{14}$$

with a similar reality condition on $A^{\rm in}_{lm}(\omega)$ and $C^{\rm out}_{lm}(\omega)$. The situation in which we are interested is a Schwarzschild space-time plus a non-vanishing perturbation of the scalar field, so at some time t_0, that we take as an initial time for the subsequent evolution, $u_{lm}(t_0, r)$ is non-vanishing, and localized in space. We then ask how this perturbation will evolve in time. In general, part of the perturbation will propagate toward infinity, and part will propagate toward the BH horizon. Thus, at $r_* \to +\infty$, we will have a purely outgoing wave. We are not interested in the case where scalar radiation is impinging on the BH from infinity, and we therefore set $C^{\rm in}_{lm}(\omega) = 0$ in eq. (10), so the boundary condition at $r = +\infty$ is

$$u_{lm}(t,r) \to \int_{-\infty}^{\infty} d\omega \, A^{\rm out}_{lm}(\omega) e^{-i\omega(t-r_*)} , \qquad (r_* \to +\infty) . \tag{15}$$

Similarly, we require that nothing is coming out from the BH horizon. Thus, near the horizon we select purely incoming-wave boundary conditions

$$u_{lm}(t,r) \to \int_{-\infty}^{\infty} d\omega\, A^{\rm in}_{lm}(\omega) e^{-i\omega(t+r_*)}\,, \quad (r_* \to -\infty)\,. \tag{16}$$

To show that the boundary conditions (15) and (16) pick out some discrete values of ω, it is convenient to start from eq. (5) in the time domain and consider the situation in which, at $r_* = -\infty$, we prepare a right-moving wave-packet

$$u^0_{lm}(t,r_*) = \int_{-\infty}^{\infty} \frac{d\omega}{2\pi}\, A^0_{lm}(\omega) \exp\{-i\omega(t-r_*)\}\,, \quad (r_* \to -\infty). \tag{17}$$

This wavepacket will be partly reflected and partly transmitted by the potential $V(r_*)$. So, at $r_* = -\infty$ there will also be a reflected, left-moving, wavepacket

$$u^{\rm refl}_{lm}(t,r_*) = \int_{-\infty}^{\infty} \frac{d\omega}{2\pi}\, A^{\rm refl}_{lm}(\omega) \exp\{-i\omega(t+r_*)\}\,, \quad (r_* \to -\infty), \tag{18}$$

while at $r = +\infty$ there will be a right-moving wavepacket,

$$u^{\rm trans}_{lm}(t,r_*) = \int_{-\infty}^{\infty} \frac{d\omega}{2\pi}\, A^{\rm trans}_{lm}(\omega) \exp\{-i\omega(t-r_*)\}\,, \quad (r_* \to +\infty)\,. \tag{19}$$

Thus, in terms of the Fourier modes $u_{lm}(\omega, r_*)$, the asymptotic solution at $r_* = -\infty$ will be

$$u_{lm}(\omega, r_*) \simeq A^0_{lm}(\omega) e^{+i\omega r_*} + A^{\rm refl}_{lm}(\omega) e^{-i\omega r_*}\,, \tag{20}$$

while at $r_* = +\infty$ we will have

$$u_{lm}(\omega, r_*) \simeq A^{\rm trans}_{lm}(\omega) e^{+i\omega x}\,. \tag{21}$$

The conservation of probability requires $|A^0_{lm}(\omega)|^2 = |A^{\rm refl}_{lm}(\omega)|^2 + |A^{\rm trans}_{lm}(\omega)|^2$. In this equivalent one-dimensional scattering problem, the amplitude for reflection is

$$S_{lm}(\omega) = \frac{A^{\rm refl}_{lm}(\omega)}{A^0_{lm}(\omega)}\,. \tag{22}$$

The boundary conditions (15) and (16) correspond to setting $A^0_{lm}(\omega) = 0$ with $A^{\rm refl}_{lm}(\omega) \neq 0$, and therefore to poles of the scattering amplitude $S_{lm}(\omega)$. So, the imposition of the boundary conditions (15) and (16) selects some discrete values of ω. In the language of scattering theory, these special frequencies are the resonances of the system. These special values of ω, that we denote by $\omega_{\rm QNM}$, are in general complex, and we write them as

$$\omega_{\rm QNM} \equiv \omega_R - i\frac{\gamma}{2}\,. \tag{23}$$

This defines the normal-mode frequency of the Schwarzschild BH. For physical reasons, we must have $\gamma > 0$,[1] corresponding to the fact that these normal-mode excitations are damped. To emphasize that these normal modes have a complex

[1] With the convention for the Fourier transform $F(t) = \int_{-\infty}^{\infty} \frac{d\omega}{2\pi}\, \tilde{F}(\omega) e^{-i\omega t}$.

frequency, one rather talk of *quasi-normal* modes. Of course, in any realistic macroscopic system the normal mode frequencies always have an imaginary part, because of dissipation. However, in normal macroscopic bodies the mechanisms responsible for dissipation, and therefore for ω_I, are partly independently of the mechanisms giving rise to rigidity, i.e. to ω_R, and we can tune the parameters of the system, or external parameters such as the temperature, so that $|\omega_I| \ll \omega_R$. In contrast, for BHs ω_R and ω_I are determined simultaneously by the same equation, and are both a consequence of gravity. There is no parameter that we can tune to achieve $|\omega_I| \ll \omega_R$.

The form (23) of the QNM frequencies has a peculiar consequence on the spatial dependence of the function describing a quasi-normal mode (its "wavefunction", in the equivalent Schrödinger problem). By definition, at $r_* \to \pm\infty$, the quasi-normal modes satisfy the boundary conditions (15) and (16), i.e.

$$u_{lm}(\omega, r_*) \propto e^{i\omega|r_*|} = e^{i\omega_R|r_*|}e^{+\gamma|r_*|/2}\,, \qquad (r_* \to \pm\infty)\,. \tag{24}$$

Since $\gamma > 0$, the quasi-normal modes diverge exponentially, both at infinity and at the horizon! This is a clear indication of the fact that QNM behave quite differently from the usual normal modes. First of all, a QNM cannot represent a physical state of the system at a given time, over all of space, since at any given time it carries an infinite energy. Rather, it can at most describe the behavior of $u_{lm}(t, r_*)$ at sufficiently large values of t, at a *fixed* value of r_*. The larger the value of $|r_*|$, the larger is also the value of time at which this asymptotic behavior sets in, so the exponentially growing factor $e^{+\gamma|r_*|/2}$ is always compensated by the time dependence $e^{-\gamma t/2}$. Another related aspect is that quasi-normal modes do not form a complete set, see [8] for full details.

2.2 Tensor perturbations in a BH background

The above analysis refers to a BH space-time perturbed by the excitation of a scalar field. We can now generalize it to perturbations of the metric itself. In this case we consider the metric $g_{\mu\nu} = \bar{g}_{\mu\nu} + h_{\mu\nu}$, where $\bar{g}_{\mu\nu}$ is the Schwarzschild metric, and $h_{\mu\nu}$ a gravitational perturbation. The treatment is conceptually very similar to that of a scalar field, except for a number of technical complications related to the tensor nature of $h_{\mu\nu}$ and to diffeomorphism invariance. Full details will be found again in [8], and here we only summarize the main points. First of all, the expansion is spherical harmonics given in eq. (4) must be replaced by an expansion in tensor spherical harmonics. Then one finds that the metric perturbations can be separated into polar and axial perturbations,

$$h_{\mu\nu}(x) = h^{\rm pol}_{\mu\nu}(x) + h^{\rm ax}_{\mu\nu}(x)\,. \tag{25}$$

For a Schwarzschild BH, to linear order in $h_{\mu\nu}$, the perturbation equations for polar and axial perturbations do not mix. The linearized theory is invariant under infinitesimal coordinate transformations

$$x^\mu \to x'^\mu = x^\mu + \xi^\mu(x)\,. \tag{26}$$

Under this transformation the background metric $\bar{g}_{\mu\nu}$ is invariant while, to linear order in $\bar{D}_\mu\xi_\nu$, $h_{\mu\nu}$ transforms as $h_{\mu\nu}(x) \to h'_{\mu\nu}(x')$, where

$$h'_{\mu\nu}(x) = h_{\mu\nu}(x) - (\bar{D}_\mu\xi_\nu + \bar{D}_\nu\xi_\mu)\,. \tag{27}$$

This expresses the gauge invariance of the spin-2 field $h_{\mu\nu}$ on the fixed background $\bar{g}_{\mu\nu}$. The next step is then to make use of this gauge freedom, to get rid of some degrees of freedom. When perturbing over a BH space-time there is a convenient gauge choice, known as the Regge-Wheeler (RW) gauge. Using this gauge, and the explicit form of the tensor spherical harmonics, one finds that the most general metric of a perturbed Schwarzschild black hole, $g_{\mu\nu} = \bar{g}_{\mu\nu} + h_{\mu\nu}$, can be written as

$$\begin{aligned} g_{\mu\nu}dx^\mu dx^\nu &= -A(r)\left[1-\sum_{l=0}^{\infty}\sum_{m=-l}^{l} H_{lm}^{(0)}Y_{lm}\right]dt^2 + 2dtdr\left[\sum_{l=1}^{\infty}\sum_{m=-l}^{l} H_{lm}^{(1)}Y_{lm}\right] \\ &+B(r)dr^2\left[1+\sum_{l=0}^{\infty}\sum_{m=-l}^{l} H_{lm}^{(2)}Y_{lm}\right] + r^2(d\theta^2+\sin^2\theta d\phi^2)\left[1+\sum_{l=2}^{\infty}\sum_{m=-l}^{l} K_{lm}Y_{lm}\right] \\ &-2dtd\theta\frac{1}{\sin\theta}\left[\sum_{l=2}^{\infty}\sum_{m=-l}^{l} h_{lm}^{(0)}\,\partial_\phi Y_{lm}\right] + 2dtd\phi\sin\theta\left[\sum_{l=2}^{\infty}\sum_{m=-l}^{l} h_{lm}^{(0)}\,\partial_\theta Y_{lm}\right] \\ &-2drd\theta\frac{1}{\sin\theta}\left[\sum_{l=1}^{\infty}\sum_{m=-l}^{l} h_{lm}^{(1)}\,\partial_\phi Y_{lm}\right] + 2drd\phi\sin\theta\left[\sum_{l=1}^{\infty}\sum_{m=-l}^{l} h_{lm}^{(1)}\,\partial_\theta Y_{lm}\right], \end{aligned} \tag{28}$$

where $A(r)$ and $B(r)$ are given in eq. (3). The functions $H^{(0)}, H^{(1)}, H^{(2)}$ and K describe polar perturbations, while $h^{(0)}$ and $h^{(1)}$ describe axial perturbations.

The next step is to show that the full set of perturbation equations for these functions can be reduced to a single master equation in the polar sector and a single master equation in the axial sector. In the axial sector one introduces the Regge-Wheeler function

$$Q_{lm}(t,r) = \frac{1}{r}A(r)h_{lm}^{(1)}(t,r)\,, \tag{29}$$

Then one finds that $\tilde{Q}_{lm}(\omega, r)$ satisfies an equation very similar to eq. (9)

$$\frac{\partial^2}{\partial r_*^2}\tilde{Q}_{lm} + \left[\omega^2 - V_l^{\rm RW}(r)\right]\tilde{Q}_{lm} = 0\,, \tag{30}$$

where as usual $r = r(r_*)$ is obtained inverting eq. (7), and

$$V_l^{\rm RW}(r) = A(r)\left[\frac{l(l+1)}{r^2} - \frac{3R_S}{r^3}\right] \tag{31}$$

is the Regge-Wheeler potential. Equation (30) is called the *Regge-Wheeler equation*. The RW potential is qualitatively very similar to the potential found for scalar perturbations. More generally, on the right-hand side we also have a source term that comes from the linearization of the energy-momentum tensor. This source term is important to study the amplitude of the excitation of the quasi-normal modes in response to a specific perturbations. However, for determining the quasi-normal mode frequencies we can set the source term to zero. Given the solution for $\tilde{Q}_{lm}$, and hence for $h_{lm}^{(1)}(t,r)$, the remaining perturbation equations determine the other functions describing axial perturbations.

Similarly, for polar perturbations all dynamical equations collapse to a single equation for a master function $\tilde{Z}_{lm}(\omega, r)$, that satisfies the *Zerilli equation*

$$\frac{\partial^2}{\partial r_*^2}\tilde{Z}_{lm} + \left[\omega^2 - V_l^{\rm Z}(r)\right]\tilde{Z}_{lm} = 0\,, \tag{32}$$

where again we have set to zero the source term. The Zerilli potential is

$$V_l^{\rm Z}(r) = A(r)\,\frac{2\lambda^2(\lambda+1)r^3 + 6\lambda^2 M r^2 + 18\lambda M^2 r + 18M^3}{r^3(\lambda r + 3M)^2}\,, \tag{33}$$

where $\lambda = (l-1)(l+2)/2$. Again, this potential is qualitatively very similar to the potential for scalar field.

Thus, BH quasi-normal modes can be defined exactly as we have done above for the scalar field, both in the axial and in the polar sector. A remarkable result (valid only for non-rotating BHs) is that, despite the different form of the potentials, the Regge-Wheeler and the Zerilli equations have exactly the same spectrum. This can be shown as follows. Suppose that two operators L_1 and L_2 are related by the relation

$$DL_1 = L_2 D\,, \tag{34}$$

where D is another operator. Let ψ by an eigenfunction of L_1, $L_1\psi = \xi\psi$. Then eq. (34) gives $L_2(D\psi) = D(L_1\psi) = \xi(D\psi)$, so for each eigenfunction ψ of L_1 there is an eigenfunction $(D\psi)$ of L_2 with the same eigenvalue. We now take as L_1 the Zerilli operator for the l-th multipole

$$(L_1)_l = \frac{d^2}{dr_*^2} - V_l^{\rm Z}\,, \tag{35}$$

and as L_2 the Regge-Wheeler operator,

$$(L_2)_l = \frac{d^2}{dr_*^2} - V_l^{\rm RW}\,. \tag{36}$$

Then, one can check that eq. (34) admits a solution of the form

$$D_l = \frac{d}{dr_*} - g_l(r)\,, \tag{37}$$

for some function $g_l(r)$.

Several techniques have been developed for computing numerically the frequencies and damping times of the quasi-normal modes. From Table 1 we see that the least damped mode emits GWs at a frequency $f = \omega_R/(2\pi)$ given by

$$f \simeq \frac{0.747}{2\pi R_S} \simeq 12\,{\rm kHz}\,\left(\frac{M_\odot}{M}\right)\,. \tag{38}$$

Thus, for a $10M_\odot$ BH we get $f \sim 1$ kHz, while a supermassive BH with $M = 10^6 M_\odot$ rings at $f \sim 10$ mHz. The ringdown signal vanishes exponentially with a characteristic time $\tau = 1/|\omega_I|$ which, for the least damped mode, is

$$\tau \simeq \frac{R_S}{0.178c} \simeq 5.5\times 10^{-5}\,{\rm s}\,\left(\frac{M}{M_\odot}\right)\,. \tag{39}$$

Table 1: The frequencies of the QNM of a Schwarzschild BH, for $l = 2$ and for $l = 3$, in units $R_S/c = 1$ (data from [21]).

	$l = 2$	$l = 3$
n	(ω_R, ω_I)	(ω_R, ω_I)
1	(0.747343, −0.177925)	(1.198887, −0.185406)
2	(0.693422, −0.547830)	(1.165288, −0.562596)
3	(0.602107, −0.956554)	(1.103370, −0.958186)
4	(0.503010, −1.410296)	(1.023924, −1.380674)
5	(0.415029, −1.893690)	(0.940348, −1.831299)
10	(0.126527, −4.605289)	(0.647366, −4.290798)
50	(0.151216, −24.693716)	(0.134153, −24.119329)

Thus, the ringdown signal from a $10M_\odot$ BH vanishes exponentially in a time of order the millisecond, while a supermassive BH with M of order a few $10^6 M_\odot$ rings for a few minutes.

2.3 Kerr black holes

The above discussion only refers to perturbations of non-rotating BHs. For application to GW astrophysics we need however to study perturbations of the Kerr solution. This introduces an extra layer of technical complexity, leading to the Teukolsky equation. Once again, full details will be presented in [8]. The effect of rotation is to remove the degeneracy of the frequency with respect to the quantum number m. For GW emission the most relevant mode is the mode with $n = 1, l = m = 2$. The spin S of a Kerr BH defines a dimensionless parameter

$$\hat{a} \equiv \frac{S}{GM^2}\,. \tag{40}$$

For the mode $n = 1, l = 2, m = 2$, the dependence of the frequency on $\hat{a}$ can be fitted to better than 5% over a range $\hat{a} \in [0, 0.99]$ by the formula

$$GM(\omega_R)_{n=1,l=2,m=2} \simeq 1.5251 - 1.1568(1 - \hat{a})^{0.1292}\,, \tag{41}$$

while for the imaginary part, defining the quality factor,

$$Q_{nlm} \equiv \frac{(\omega_R)_{nlm}}{2|(\omega_I)_{nlm}|}\,, \tag{42}$$

one finds

$$Q_{n=1,l=2,m=2} \simeq 0.700 + 1.4187(1 - \hat{a})^{0.4990}\,. \tag{43}$$

Similarly, for the mode $n = 1, l = 2, m = 0$ an accurate fitting formula is [19, 20]

$$GM(\omega_R)_{n=1,l=2,m=0} \simeq 0.4437 - 0.0739(1 - \hat{a})^{0.3350}\,, \tag{44}$$

$$Q_{n=1,l=2,m=0} \simeq 4.000 - 1.9550(1 - \hat{a})^{0.1420}\,. \tag{45}$$

2.4 BH quasi-normal modes and GW150914

It is quite exciting that now, with the first observations of coalescences of BH-BH binaries, we can start to investigate these QNMs observationally. To observe this ringing of space-time is by itself a remarkable fact. Furthermore, with the improved sensitivity expected in the near future by advanced detectors, we can hope to test quantitatively the predictions of GR for the BHs QNM. This would be a remarkable test of GR in strong fields.[2]

As as been discussed by Thibault Damour in the previous lecture in this seminar, the waveform for a BH-BH coalescence can be roughly divided into a long inspiral phase, followed by merger and ringdown. The full evolution is by now under full control thanks both to analytic breakthroughs such as the EOB technique [23, 24] and breakthroughs in numerical relativity [25–27]. The two methods complement each other very well. Numerical relativity provides more accurate waveforms, but a single simulation typically takes months on a supercomputer. For detecting and subsequently analyzing the signal at GW interferometers one needs to finely scan the space of parameters parametrized by the masses and spins of the BHs. Even assuming spins parallel to the orbital angular momentum, as done in the LIGO discovery paper [2, 5] still requires the use of about 250'000 templates, which can be efficiently generated by tuning the analytic EOB waveform to numerical relativity. The resulting templates are referred as "EOBNR" waveforms. Much work has been done recently to implement efficiently these waveform in the LIGO data analysis pipeline, to include spin, etc., see [8] for a full list of references.

The final part of these waveforms is the "ringdown" phase, given by the oscillation of the final BH in its quasinormal modes, and the signal is a superposition of damped sinusoids. As mentioned above, for GW emission the most relevant mode is the mode $n = 1, l = 2, m = 2$, and its frequency $(\omega_R)_{122}$ and damping time τ_{122} are given in eqs. (41) and (42). Keeping for simplicity only this mode, in the ringdown phase the waveform has the form

$$h_+(t) = \mathcal{A}\, e^{-(t-t_{\rm M})/\tau_{122}} \cos[(\omega_R)_{122}(t - t_{\rm M}) + \mathcal{B}]\,. \tag{46}$$

where $t_{\rm M}$ marks the end of the merger phase and this analytic form holds for t sufficiently larger than t_M. The constants constants $\mathcal{A}$ and $\mathcal{B}$ are determined from the full numerical relativity evolution or, within the EOB approach, by matching this solution to the EOB solution from the merger phase, by requiring the continuity of $h_+(t)$ and of dh_+/dt at $t = t_{\rm M}$. It is in principle straightforward to improve the result including higher quasinormal modes.

One can now try to test this behavior against the observations. This test can be performed with GW150914, since, given the masses of the initial BHs in this system, the peak frequency of its GW amplitude falls in the frequency range where the LIGO detectors have their best sensitivity, and it still has a relatively large amplitude even in the ringdown regime. In contrast the second detected even, GW151226, because of the smaller masses of the initial BHs and a similar distance, compared to GW150914, has a smaller amplitude, and its ringdown phase is not really visible.

[2] It is also quite interesting to ask whether this would be an unambiguous proof of the fact that we are indeed observing BHs, rather than other exotic compact objects that have been considered in the literature (e.g., boson stars), which would not have a horizon. Actually, this is a non-trivial question, because the initial part of the ringdown signal turns out to depend basically on the existence of a light-ring, rather than of a horizon, and could be mimicked by objects without a horizon, while the late-time ringdown signal would be different, see [22].

With GW150914 we can test the prediction of GR for the frequency and damping times of the lowest QNM as follows. The mass and spin of the final BH are obtained from the reconstruction of the full waveform, identifying the EOBNR template that matches best the signal. Then, as we have seen, GR predicts the frequency and the decay time of the BH quasi-normal modes (QNMs) and in particular of the dominant, least-damped, QNM, see eqs. (41) and (43). We can then compare this prediction with the damped oscillating behavior of the final part of the waveform. There is however a certain ambiguity as to the exact definition of the 'final part' of the waveform, which should be compared to the prediction (46). If we denote by t_M the time of merger, we can compare the predicted ringdown waveform to the data starting from time $t_0 = t_M + \Delta t$. If we take Δt too small the signal is however still dominated by the merger phase, rather than by ringdown. If we take Δt too large, we are indeed in the region dominated by ringdown, but the signal vanishes exponentially, so the accuracy of the test quickly degrades. This study has then been performed in the LIGO/Virgo paper on tests of GR [28] (see in particular their Fig. 4), for different Δt, comparing each time the frequency and decay time of the dominant QNM, extracted by fitting the final part of the waveform to a damped sinusoid, to the values obtained determining the final mass and spin from the full waveform and then using the prediction (41) and (43) of BH perturbation theory. The result is that, starting from $\Delta t = 3$ ms, the 90% confidence region obtained by fitting the waveform to a damped sinusoid overlaps with the 90% confidence region obtained from BH perturbation theory. Thus, within the available accuracy, the GR prediction for the frequency and decay time of the least-damped BH quasi-normal mode is consistent with the data. A more stringent test would be obtained if, with higher SNR, one could extract from the waveform the frequency and decay time of two QNMs, since from these informations one could obtain an independent reconstruction of the mass and spin of the final BH, and compare with the one obtained from the full waveform. Such tests should be possible in the near future with the continuous improving of the sensitivity of the advanced interferometers. Ideally, beside the mass and spin of the final BH, one would like to reconstruct from the QNM even some higher multipole moments, which would allow us to test the no-hair theorem of GR. Such tests might in principle be done with the detection of extreme mass ratio inspirals (EMRI) at a space-borne interferometer such as (e)LISA.

3 GWs and cosmology

As a second topic, we discuss stochastic background of GWs of cosmological origin (we follow the discussion in refs. [7, 8, 29]). Once again, this is a possible signal that would carry information unaccessible with other probes, and in particular it could allow us to probe early Universe cosmology down to a primordial epoch unaccessible to electromagnetic observations. The basic reason is that particles decouple from the primordial plasma when the rate Γ of the processes that maintain them in equilibrium with the rest of the plasma becomes smaller than the rate of expansion of the Universe, which is given by the Hubble parameter $H(t)$. In particular, photons decouple from baryons at a temperature $T = T_{\rm dec} \simeq 0.26$ eV. Indeed, at higher temperatures photons are kept in equilibrium with electrons by Compton scattering, and the electrons are tightly coupled to the protons via Coulomb scattering. At recombinations, most free electrons combine with protons to form hydrogen atoms

and the number density of free electrons, n_e, drops. Thus, photons decouple from electrons (and hence from protons) when $\Gamma(T)$ drops below $H(T)$, where $\Gamma(T) = \sigma_T n_e$, with σ_T given by the Thomson cross-section and n_e the number density of the remaining free electrons. The condition $\Gamma(T_{\rm dec}) = H(T_{\rm dec})$ gives the decoupling temperature

$$T_{\rm dec} \simeq 0.26\,{\rm eV}\,, \tag{47}$$

corresponding to a redshift

$$z_{\rm dec} \simeq 1090\,. \tag{48}$$

At this point, photons start to propagate freely. This red-shift therefore defines the last scattering surface of the CMB photons. Thus, the observation of the CMB anisotropies give us a snapshot of the Universe at this epoch.

Let us next compute the epoch when neutrinos decouples from the primordial plasma. For massless or light particles in equilibrium at a temperature T, the number density $n \sim T^3$. For neutrinos equilibrium is maintained by weak processes such as electron-neutrino scattering and at energies below the W mass, the cross section $\sigma \sim G_F^2 \langle E^2\rangle \sim G_F^2 T^2$ where G_F is the Fermi constant and $\langle E^2\rangle$ is the average energy squared. The Hubble parameter during the radiation dominated era is related to the temperature by $H \sim T^2/M_{\rm Pl}$. Therefore

$$\left(\frac{\Gamma}{H}\right)_{\rm neutrino} \sim \frac{G_F^2 T^5}{T^2/M_{\rm Pl}} \simeq \left(\frac{T}{1{\rm MeV}}\right)^3\,. \tag{49}$$

Even the weakly interacting neutrinos, therefore, cannot carry informations on the state of the Universe at temperatures larger than approximately 1 MeV.

If we repeat the above computation for gravitons, the Fermi constant G_F is replaced by Newton constant $G = 1/M_{\rm Pl}^2$, where $M_{\rm Pl} \sim 10^{19}$ GeV is the Planck mass. Thus, at energies below $M_{\rm Pl}$,

$$\left(\frac{\Gamma}{H}\right)_{\rm graviton} \sim \left(\frac{T}{M_{\rm Pl}}\right)^3\,. \tag{50}$$

Gravitons are therefore decoupled below the Planck scale. It follows that relic gravitational waves are a potential source of informations on very high-energy physics. Gravitational waves produced in the very early Universe have not lost memory of the conditions in which they have been produced, as it happened to all other particles, but still retain in their spectrum, typical frequency and intensity, important informations on the state of the very early Universe, and therefore on physics at correspondingly high energies, which cannot be accessed experimentally in any other way.

In order to discuss stochastic backgrounds of GWs we need to introduce some definitions. The metric perturbation h_{ij} can be written as a superposition of plane waves coming from all directions $\hat{\mathbf{n}}$, as

$$h_{ij}(t,\mathbf{x}) = \sum_{A=+,\times} \int_{-\infty}^{\infty} df \int d^2\hat{\mathbf{n}}\, \tilde{h}_A(f,\hat{\mathbf{n}})\, e_{ij}^A(\hat{\mathbf{n}})\, e^{-2\pi i f(t-\hat{\mathbf{n}}\cdot\mathbf{x}/c)}\,. \tag{51}$$

We work in the TT gauge, so $h_i^i =$ and $\partial^j h_{ij} = 0$. The polarization tensors $e_{ij}^A(\hat{\mathbf{n}})$ are given by

$$e_{ij}^+(\hat{\mathbf{n}}) = \hat{\mathbf{u}}_i\hat{\mathbf{u}}_j - \hat{\mathbf{v}}_i\hat{\mathbf{v}}_j\,, \quad e_{ij}^\times(\hat{\mathbf{n}}) = \hat{\mathbf{u}}_i\hat{\mathbf{v}}_j + \hat{\mathbf{v}}_i\hat{\mathbf{u}}_j\,, \tag{52}$$

with $\hat{\mathbf{u}}, \hat{\mathbf{v}}$ unit vectors orthogonal to the propagation direction $\hat{\mathbf{n}}$ and to each other. In a stochastic background, the amplitudes $\tilde{h}_A(f, \hat{\mathbf{n}})$ are random variables, characterized statistically by their ensemble averages. Assuming that the stochastic background is stationary, isotropic, unpolarized and Gaussian (all assumptions that, in a second stage, it will be interesting to relax), it is fully characterized by its two-point function, which can be written as

$$\langle \tilde{h}^*_A(f, \hat{\mathbf{n}}) \tilde{h}_{A'}(f', \hat{\mathbf{n}}') \rangle = \delta(f - f') \, \frac{\delta^2(\hat{\mathbf{n}}, \hat{\mathbf{n}}')}{4\pi} \, \delta_{AA'} \, \frac{1}{2} S_h(f) \, . \tag{53}$$

The function $S_h(f)$ is called the spectral density of the stochastic background. The energy density is given by the standard formula (see e.g. eq. (1.135) of [7])

$$\rho_{\rm gw} = \frac{1}{32\pi G} \langle \dot{h}_{ij} \dot{h}^{ij} \rangle \, . \tag{54}$$

(Recall that here we are using units $c = 1$). Inserting here the expression (51) for h_{ij} one finds that, for a stochastic background, $\rho_{\rm gw}$ can be written as an integral over frequencies, as

$$\rho_{\rm gw} \equiv \int_{f=0}^{f=\infty} d(\log f) \, \frac{d\rho_{\rm gw}}{d \log f} \, . \tag{55}$$

where

$$\frac{d\rho_{\rm gw}}{d \log f} = \frac{\pi c^2}{2G} f^3 S_h(f) \, . \tag{56}$$

In cosmology there is a very natural unit of energy density, that is, the energy density needed for closing the Universe. This critical energy density is

$$\rho_c = \frac{3H_0^2}{8\pi G} \, , \tag{57}$$

where H_0 is the present value of the Hubble expansion rate, $H_0 = h_0 \times 100$ km s^{-1} Mpc^{-1}, where $h_0 \simeq 0.70$ parametrizes the existing experimental uncertainty. It is then natural to normalize $\rho_{\rm gw}$ to ρ_c, defining

$$\Omega_{\rm gw}(f) \equiv \frac{1}{\rho_c} \frac{d\rho_{\rm gw}}{d \log f} = \frac{4\pi^2}{3H_0^2} \, f^3 S_h(f) \, . \tag{58}$$

It is actually customary to use the quantity $h_0^2 \Omega_{\rm gw}(f)$, which is independent on the observational uncertainty on h_0. The factor f^3 in eq. (58) has important consequences for the limits that can be obtained observationally on $\Omega_{\rm gw}(f)$ at different frequencies. The spectral density of the signal, $S_h(f)$ is the quantity that will have to be compared to the spectral density of the noise of a detector, $S_n(f)$ (in a non-trivial way, when performing the correlation between two or more detectors), to determine the minimum value of $S_h(f)$ that can be detected. Of course, the experimental challenges for building detectors working on different range of frequencies are very different. However, to determine the sensitivity to $\Omega_{\rm gw}(f)$, in general the dominant effect is given by the f^3 factor in front of eq. (58). Indeed, the range of frequencies explored by GW experiments is huge. CMB experiments are potentially sensitive to GWs with wavelengths comparable to the present horizon size of the Universe, corresponding to frequencies f of order $10^{-18} - 10^{-17}$ Hz. In contrast, pulsar timing arrays are sensitive to stochastic backgrounds of GWs with a frequency

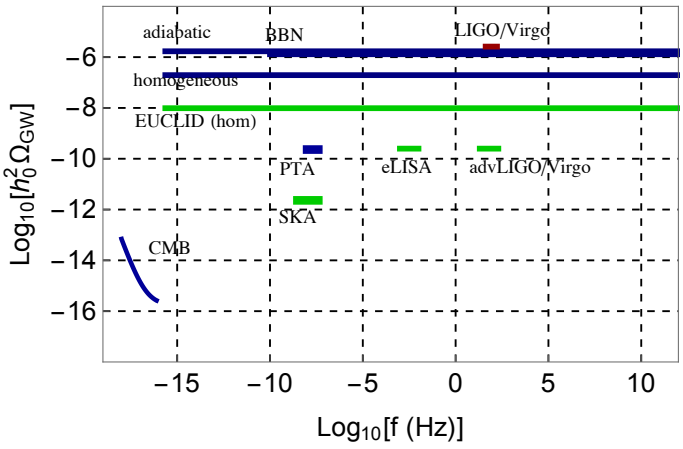

Figure 2: Observational limits on $h_0^2\Omega_{\rm gw}(f)$ (blue lines) and expected limits that should be obtained from future observations (green lines).

of the order of the inverse observation time span, which is about 10 years, leading to f of order 10^{-9} Hz. Ground-based GW interferometers have their best sensitivity at $f \sim 10^2$ Hz. Thus, the factor f^3 in eq. (58) can make a huge difference. To obtain a good sensitivity to $\Omega_{\rm gw}(f)$ at high frequencies, one should be able to build a detector with a much smaller noise spectral density.

3.1 Existing limits

Fig. 2 shows existing and forecasted limits on $h_0^2\Omega_{\rm gw}(f)$. Observe that the horizontal axis covers a huge range of frequencies. On the lower end, frequencies $f \sim 10^{-18}$ Hz corresponds to wavelength of order of the horizon size today. Thus, these are the longest possible wavelengths (and hence the smallest possible frequencies) which are observable as GWs. Stochastic backgrounds of GWs with such small frequencies are indeed in principle detectable through their effects on CMB temperature anisotropies and polarization. The upper end of the horizontal axis, $f \sim 10^{12}$ Hz, would correspond to the frequency of a graviton produced when the temperature of the Universe was close to the Planck mass, redshifted up to the present epoch neglecting any possible inflationary phase in between. These are the highest possible frequencies that one can consider. More generally, consider the GWs produced by some cosmological mechanism, when the Hubble parameter had a value H_*. Then their characteristic wavelength λ_* will be of order H_*^{-1}. More precisely, we will have

$$\lambda_* = \epsilon H_*^{-1}\,, \tag{59}$$

where $\epsilon \leq 1$ because of causality. During RD, $H_*^2 = (8\pi/3)G\rho_{\rm rad}$, so

$$H_*^2 = \frac{8\pi^3 g_* T_*^4}{90 M_{\rm Pl}^2}\,, \tag{60}$$

where T_* and g_* are the corresponding values of the temperature and of the effective number of relativistic species. Then, after redshifting $f_* \equiv H_*/\epsilon$ down to the present

epoch, we find the the present value of the GW frequency, f_0, is given by

$$f_0 \simeq 1.67 \times 10^{-7} \, \frac{1}{\epsilon} \left(\frac{T_*}{1\text{GeV}} \right) \left(\frac{g_*}{106.75} \right)^{1/6} \text{Hz} \, . \tag{61}$$

This gives a first estimate of the typical frequency, today, of the GWs produced by a cosmological mechanis acting when the temperature of the Universe was T_*.

We refer to [8] for a detailed discussion and derivation of the bounds shown in Fig. 2. Here we just observe that the long horizontal blue lines correspond to bounds on the total energy density $\rho_{\rm gw}$ at different epoch, hence are bounds on the integral of $h_0^2\Omega_{\rm gw}(f)$ over the range of frequencies that were inside the horizon at the relative epoch. An example is given by the Big-Bang Nucleosynthesis (BBN) bound. The outcome of BBN is fixed by a balance between the nuclear reaction rates and the expansion rate of the Universe, which in turn is controlled by the total energy density at time of BBN. The BBN bound then comes from the requirement that there cannot be too much extra energy density at time of nucleosynthesis, compared to that predicted by the particle content of the Standard Model, since otherwise this would eventually spoil the success of the BBN prediction for the abundance of the light elements. The bound has the form

$$\int_{f=f_{\rm BBN}}^{f=\infty} d(\log f) \; h_0^2\Omega_{\rm gw}(f) < 1.3 \times 10^{-6} \left(\frac{N_{\rm eff} - 3.046}{0.234} \right) \, . \tag{62}$$

The quantity $N_{\rm eff}$ is called the 'effective number of neutrino species", and in the Standard Model has the value $N_{\rm eff} \simeq 3.046$ (where the difference from the value $N_{\rm eff} = 3$ reflecting the three neutrino species is due to the fact that neutrino decoupling is not instantaneous, and to finite temperature QED effects [30]). The most recent bound on $N_{\rm eff}$ is $N_{\rm eff} - 3.046 < 0.234$, obtained by combining measurements of primordial abundances of light elements with the determination by *Planck* of the baryon-to-photon ratio [31]. Note that this is a bound on the total energy density in gravitational waves, integrated over all frequencies. However, only the frequencies that were inside the horizon at time of BBN contribute to the expansion of the Universe. The BBN bound is therefore a bound on the integral of $h_0^2\Omega_{\rm gw}(f)$ for $f > f_{\rm BBN}$. From the mathematical point of view one could of course imagine a function $h_0^2\Omega_{\rm gw}(f)$ with a very narrow peak in $h_0^2\Omega_{\rm gw}(f)$ at some frequency f, with a peak value larger than the right-hand side of eq. (62), but sufficiently narrow so that its contribution to the integral could be small enough. However, all typical cosmological production mechanisms rather give a spectrum that, even in the most peaked case, such as phase transitions, still covers at least one decade in frequency. For such spectra, we can transform the bound in eq. (62) on a bound on $h_0^2\Omega_{\rm gw}(f)$, requiring that, if the integral cannot exceed a given values, even its positive definite integrand $h_0^2\Omega_{\rm gw}(f)$ cannot exceed it over an appreciable interval of frequencies $\Delta \log f \sim 1$, so we can impose

$$h_0^2\Omega_{\rm gw}(f) < 1.3 \times 10^{-6} \left(\frac{N_{\rm eff} - 3.046}{0.234} \right) \, , \qquad (\text{for } f > f_{\rm BBN}). \tag{63}$$

This is the meaning of the bound marked as "BBN" in Fig. 2. A similar integral bounds come from the limits on extra radiation at the CMB epoch, and differs depending on whether tensor perturbations are homogeneous or adiabatic [32].

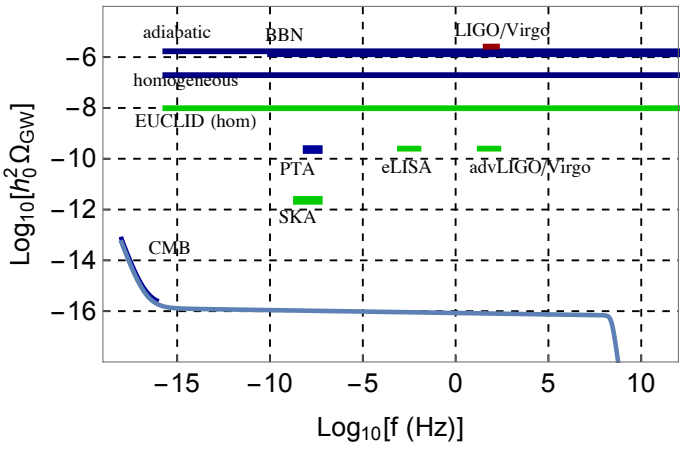

Figure 3: The prediction for $h_0^2\Omega_{\rm gw}(f)$ from single-field slow-roll inflation with a tensor-to-scalar ratio $r = 0.1$, compared to the observational bounds.

The figure also shows the direct upper limits found by CMB experiments, by pulsar timing arrays, and by the LIGO/Virgo collaboration with the initial interferometers, see again [8] for detailed derivations and discussions.

3.2 Production mechanisms

The crucial question is which mechanisms could produce sizable stochastic backgrounds of GWs, and at which frequencies. In the last decades there has been much activity in this direction. One of the best studied mechanisms is the production of GWs because of amplification of quantum vacuum fluctuations in single-field slow-roll inflation. This gives a result from $h_0^2\Omega_{\rm gw}(f)$ whose functional form is fixed, with a $1/f^2$ behavior at very low frequencies, $f < f_{\rm eq} \simeq 1.6 \times 10^{-17}\,{\rm Hz}$ (corresponding to frequencies that re-entered the horizon during matter dominance), followed by a long almost flat part, $h_0^2\Omega_{\rm gw}(f) \propto f^{-r/8}$, where is the tensor-to-scalar ratio, which is bounded observationally to $r < 0.1$. The overall amplitude depends indeed on r, and in Fig. 3 we show it for the value $r = 0.1$ that saturates the CMB limit. Proposed satellite experiments such as COrE and LiteBIRD aim at detecting primordial GWs from B mode polarization, detecting values of r as low as $r \simeq 0.001$. In contrast, we see that the signal is too small for the present and near-future generations of ground-based and space-borne detectors.

Several other mechanism have been discussed in the literature. Alternatives to inflation can produce spectra for $h_0^2\Omega_{\rm gw}(f)$ growing with f, giving larger signals at interferometer frequencies (an example is provided by the pre-big-bang scenario inspired by string theory [33, 34], which predicts a spectrum $h_0^2\Omega_{\rm gw}(f) \propto f^3$ at low frequencies, which then saturates at the level of the BBN bound [35,36]). First-order phase transitions in the early Universe would produce GWs through the nucleation and collision of bubbles [37–40]. For a first-order phase transition at the electrowak scale (which requires extensions of the Standard Model) the signal could be detectable at eLISA, depending on the parameters of the model [41–44]. Cosmic strings, which again could be produced in extensions of the Standard Model, would produce stochastic backgrounds of GWs through oscillating string loops [45] as well

as from bursts due to cusps and kinks [46,47], in the frequencies of ground-based and space-borne interferometers, as well as of pulsar timing arrays. Again, we refer to [8] for detailed discussions and full reference list. Clearly, a detection of a stochastic GW background of cosmological origin would open a window on the Universe, and on high-energy physics, that would be quite unique.

References

[1] Abbott, B. P. *et al.*: [LIGO Scientific Collaboration and Virgo Collaboration]. Observation of Gravitational Waves from a Binary Black Hole Merger. Phys. Rev. Lett. **116**, 061102 (2016a). [arXiv:1602.03837 [gr-qc]].

[2] Abbott, B. P. *et al.*: [LIGO Scientific Collaboration and Virgo Collaboration]. GW150914: First results from the search for binary black hole coalescence with Advanced LIGO. Phys. Rev. D **93**, 122003 (2016c). [arXiv:1602.03839 [gr-qc]].

[3] Abbott, B. P. *et al.*: [LIGO Scientific Collaboration and Virgo Collaboration]. Properties of the binary black hole merger GW150914. Phys. Rev. Lett. **116**, 241102 (2016d). [arXiv:1602.03840 [gr-qc]].

[4] Abbott, B. P., *et al.*: [LIGO Scientific Collaboration and Virgo Collaboration]. Observing gravitational-wave transient GW150914 with minimal assumptions. Phys. Rev. D **93**, 122004 (2016g). [arXiv:1602.03843 [gr-qc]].

[5] Abbott, B. P., *et al.*: [LIGO Scientific Collaboration and Virgo Collaboration]. GW151226: Observation of Gravitational Waves from a 22-Solar-Mass Binary Black Hole Coalescence. Phys. Rev. Lett. **116**, 241103 (2016m). [arXiv:1606.04855 [gr-qc]].

[6] Abbott, B. P., *et al.*: [LIGO Scientific Collaboration and Virgo Collaboration]. Binary Black Hole Mergers in the first Advanced LIGO Observing Run. (2016n). [arXiv:1606.04856 [gr-qc]].

[7] Maggiore, M.: *Gravitational Waves. Vol. 1: Theory and Experiments*. 554 pages, Oxford University Press, 2008.

[8] Maggiore, M.: *Gravitational Waves. Vol. 2: Astrophysics and Cosmology*. Oxford University Press, under completion.

[9] Regge, T., and Wheeler, J. A.: Phys. Rev. **108**, 1063 (1957).

[10] Zerilli, F. J.: Phys. Rev. D **2**, 2141 (1970).

[11] Vishveshwara, C. V.: Phys. Rev. D **1**, 2870 (1970).

[12] Press, W. H.: Astrophys. J. **170** L105 (1971).

[13] Teukolsky, S. A.: Astrophys. J. **185** 635 (1973).

[14] Chandrasekhar, S.: Proc. Roy. Soc. Lond. A **343**, 289 (1975).

[15] Chandrasekhar, S.: *The Mathematical Theory of Black Holes*. Oxford University Press, Oxford, (1983).

[16] Chandrasekhar, S., and Detweiler, S.: Proc. Roy. Soc. Lond. A **344**, 441 (1975).

[17] Kokkotas, K. D., and Schmidt, B. G.: Living Rev. Rel. **2**, 2 (1999).

[18] Nollert, H.-P.:. Class. Quant. Grav. **16**, R159 (1999).

[19] Berti, E., Cardoso, V., and Starinets, A. O.: Class. Quant. Grav. **26**, 163001 (2009).

[20] Berti, E., Cardoso, V., and Will, C. M.: Phys. Rev. D **73**, 064030 (2006).

[21] Leaver, E. W.: Proc. Roy. Soc. Lond. A **402**, 285 (1985).

[22] Cardoso, V., Franzin, E., and Pani, P.: Phys. Rev. Lett. **116**, 171101 (2016). Erratum: [Phys. Rev. Lett. **117** no.8, 089902] [arXiv:1602.07309 [gr-qc]].

[23] Buonanno, A., and Damour, T.: Phys. Rev. D **59** 084006 (1999).

[24] Buonanno, A., and Damour, T.: Phys. Rev. D **62** 064015 (2000).

[25] Pretorius, F.: Phys. Rev. Lett. **95**, 121101 (2005). [gr-qc/0507014].

[26] Campanelli, M., Lousto, C. O., Marronetti, P., and Zlochower, Y.: Phys. Rev. Lett. **96**, 111101 (2006).

[27] Baker, J. G., Centrella, J., Choi, D. I., Koppitz, M., and van Meter, J.: Phys. Rev. Lett. **96**, 111102 (2006). [gr-qc/0511103].

[28] Abbott, B. P. *et al.*: [LIGO Scientific Collaboration and Virgo Collaboration]. Tests of general relativity with GW150914. Phys. Rev. Lett. **116**, 221101 (2016e). [arXiv:1602.03841 [gr-qc]].

[29] Maggiore, M.: Phys. Rept. **331**, 283 (2000). [gr-qc/9909001].

[30] Mangano, G., Miele, G., Pastor, S., and Peloso, M.: Phys. Lett. B **534**, 8 (2002). [astro-ph/0111408].

[31] Ade *et al.*: [Planck Collaboration], P. A. R.: *Planck 2015 results. XIII. Cosmological parameters*. (2015a). [arXiv:1502.01589 [astro-ph.CO]].

[32] Smith, T. L., Pierpaoli, E., and Kamionkowski, M.: Phys. Rev. Lett. **97**, 021301 (2006). [astro-ph/0603144].

[33] Gasperini, M., and Veneziano, G.: . Astropart. Phys. **1**, 317 (1993a).

[34] Gasperini, M., and Veneziano, G.: Phys. Rept. **373**, 1 (2003). [hep-th/0207130].

[35] Brustein, R., Gasperini, M., Giovannini, M., and Veneziano, G.: Phys. Lett. B **361**, 45 (1995). [hep-th/9507017].

[36] Buonanno, A., Maggiore, M., and Ungarelli, C.: Phys. Rev. D **55**, 3330 (1997). [gr-qc/9605072].

[37] Kosowsky, A., Turner, M. S., and Watkins, R.: Phys. Rev. Lett. **69**, 2026 (1992a).

[38] Kosowsky, A., Turner, M. S., and Watkins, R.: Phys. Rev. D **45**, 4514 (1992b).

[39] Kosowsky, A., and Turner, M. S.: Phys. Rev. D **47**, 4372 (1993). [astro-ph/9211004].

[40] Kamionkowski, M., Kosowsky, A., and Turner, M.: Phys. Rev. D **49** 2837 (1994).

[41] Apreda, R., Maggiore, M., Nicolis, A., and Riotto, A.: Nucl. Phys. B **631**, 342 (2002). [gr-qc/0107033].

[42] Huber, S. J., and Konstandin, T.: JCAP **0809**, 022 (2008). [arXiv:0806.1828 [hep-ph]].

[43] Caprini, C., Durrer, R., Konstandin, T., and Servant, G.: Phys. Rev. D **79**, 083519 (2009). [arXiv:0901.1661 [astro-ph.CO]].

[44] Binetruy, P., Bohe, A., Caprini, C., and Dufaux, J. F.: JCAP **1206**, 027 (2012). [arXiv:1201.0983 [gr-qc]].

[45] Vilenkin, A.: Phys. Lett. B **107**, 47 (1981b).

[46] Damour, T., and Vilenkin, A.: Phys. Rev. Lett. **85**, 3761 (2000). [gr-qc/0004075].

[47] Damour, T., and Vilenkin, A.: Phys. Rev. D **64**, 064008 (2001). [gr-qc/0104026].